Rapid Communications

Self-organization in a bimotility mixture of model microswimmers

Adyant Agrawal* and Sujin B. Babu†
Department of Physics, Indian Institute of Technology Delhi, New Delhi 110016, India

(Received 1 October 2017; published 7 February 2018)

We study the cooperation and segregation dynamics in a bimotility mixture of microorganisms which swim at low Reynolds numbers via periodic deformations along the body. We employ a multiparticle collision dynamics method to simulate a two component mixture of artificial swimmers, termed as Taylor lines, which differ from each other only in the propulsion speed. The analysis reveals that a contribution of slower swimmers towards clustering, on average, is much larger as compared to the faster ones. We notice distinctive self-organizing dynamics, depending on the percentage difference in the speed of the two kinds. If this difference is large, the faster ones fragment the clusters of the slower ones in order to reach the boundary and form segregated clusters. Contrarily, when it is small, both kinds mix together at first, the faster ones usually leading the cluster and then gradually the slower ones slide out thereby also leading to segregation.

DOI: 10.1103/PhysRevE.97.020401

Introduction. The collective motility of microorganisms is quintessential in a range of biological activities [1–5]. Much insight has been gained regarding the various aggregating patterns, such as swarming, clustering, or band formation in their suspensions [4–11]. Large scale cooperative movement is seen in microorganisms which propagate by virtue of deformations along the cell body. Such swimming strategies are commonly seen in spermatozoa, *Caenorhabditis elegans* and various flagellated microswimmers [11–19]. Taylor [20] designed a simple model for such swimmers composed of small amplitude waves traveling along a two dimensional sheet and studied that two such sheets are most efficient when they beat in synchronization. The evolution of phase locking in the Taylor sheets due to hydrodynamics was analyzed later [21]. In a recent work, Münch et al. [22] formulated a generalized model of the microswimmers in question, termed as the Taylor line, which was in fact a discretized model of the Taylor sheet. Using similar models, Yang et al. have previously shown that aggregation in case of spermatozoa and flagella is a consequence of synchronization of beating waves and is hydrodynamically favorable as it reduces energy consumption in transport [23,24]. Although the dynamic clustering behavior has been studied for active particles in the case of chemotaxis [25–29], these processes also seem to occur even in the absence of cell to cell signaling or chemotaxis [9–13]. However, only a small amount of works explore the various factors leading to the dynamic clustering in such particles [6–8].

The real systems composed of swimmers have a range of different motilities. In addition, a portion of swimmers may be unhealthy or may employ atypical swimming strategies and hence immensely differ in propagating strengths. Consequently, a positive feedback between clustering and segregation was reported for a mixture of active self-propelled rods and their passive counterparts [1,30]. Also, phase separation in a mixture of active and passive Brownian particles has been intensively studied for the high activity ratio [31]. The same phenomenon was recently shown for a lower activity ratio in the case of polymer mixtures [32]. We investigate the bimotility homogeneous mixture of microswimmers which propel with the help of planar beating mechanisms in a Newtonian fluid. In contrast to previous works, here the segregation is observed even when both components comprising the mixtures are active and are exactly same in shape, size, and mass but differ in propulsion speed. Apart from the segregation dynamics, the two component system also provides information about the cooperation between the swimmers which assists aggregation. Understanding this cooperation is prerequisite to a deeper understanding of the collective motion of microswimmers.

Simulation method. In the present Rapid Communication, we consider only hydrodynamic and steric interactions between the swimmers. To model an artificial swimmer, we use the two dimensional discretized model termed as the Taylor line [22]. The Taylor line hydrodynamically interacts with the fluid using a sinusoidal bending wave which moves along the body [32]. To simulate fluid environment, multiparticle collision dynamics (MPC) is used which employs coarse-grained particles of mass $m = 1$ [33,34].

As the Taylor line is continuously pumping energy into the system, we have used MPC with Anderson thermostat and angular momentum conservation [34]. The method consists of consecutive collision and streaming steps. In the ballistic streaming step, the coordinates of the fluid particles $\{\vec{r_i}\}$ having velocity $\{\vec{v_i}\}$ are updated with integration time Dt. For the collision step, the particles are segregated into collision cells of length $a_0 = 1$ and are imparted random velocities chosen from the Gaussian distribution of variance k_BT/m such that the momentum of the cell is conserved. k_BT is taken to be unity where k_B is the Boltzmann constant and T is the temperature of the system. The position of the grid with respect to the box is randomly changed in each step so as to incorporate Galilean invariance. We have chosen the density of fluid as

*adyant2@gmail.com
†sujin@physics.iitd.ac.in

 ©2018 American Physical Society

$10m/{a_0}^3$. The unit of time is $[t] = a_0\sqrt{(m/k_BT)}$. We make use of both rigid and periodic boundary walls in this Rapid Communication. In the case of a rigid boundary, we use a $L \times L$ square and a circle of radius R as the types of wall. To mimic fluid flow at the rigid walls of a confinement, we bounce back the fluid particles crossing the walls and employ the ghost particle method in order to satisfy the no-slip (rigid) boundary condition [34].

A Taylor line consists of a sequence of N beads each of mass $10m$. The ith bead points towards the next bead with a bond vector $\overrightarrow{t_i}$. These beads interact with the nearest neighbors by two kinds of potentials. First, a Hooke's spring potential with an equilibrium distance of $l = 0.5a_0$ and a spring constant of $D = 10^6$. Second, a bending potential $V_B = \frac{\kappa}{2}\sum_{i=1}^{N-1}[\overrightarrow{t_{i+1}} - R(\alpha_i)\overrightarrow{t_i}\,]$ [22] that keeps the consecutive bond vectors aligned at an equilibrium angle of α_i with the bending rigidity κ. Here, $R(\alpha)$ is a rotation matrix that rotates a vector clockwise by an angle α. A sinusoidal wave of beating frequency ν is generated along the contour of the Taylor line by varying curvature $c(i,t) = \alpha_i/l$ spontaneously with time t and bead position i,

$$c(i,t) = b\,\sin\left[2\pi\left(\nu t + \frac{2i}{N}\right) + \phi\right], \tag{1}$$

where parameter b controls the amplitude and ϕ is the initial phase shift. The factor of 2 with i assures that the phase difference between the first and the last bead is 4π.

In order to model the interaction among various swimmers, we use a truncated Leonard-Jones potential,

$$V_I = 4\epsilon\left[\left(\frac{r_o}{r}\right)^{12} - \left(\frac{r_o}{r}\right)^{6}\right], \qquad r < 2^{1/6}r_o, \tag{2}$$

where r is the separation between the beads of different Taylor lines, r_o is taken to be equal to a_0, and $\epsilon = 13.75$ [23,24] is the strength of the potential. Using this potential along with the intraswimmer potentials, we calculate the acceleration on every bead and update their positions with integration time step $dt = 0.01Dt$. To simulate the hydrodynamic interaction between the swimmers, we make the beads participate in every collision step. This incorporates the Taylor line into the fluid environment. The Taylor lines are allowed to easily slide on the walls by implementing a bounce forward rule on the beads. We have performed simulations with a number density of $\rho = 1.5 \times 10^{-3}$. Initially, the swimmers are scattered inside MPC fluid with a random center of mass coordinate, orientation, initial phase, and direction of motion.

For the purpose of our simulations we choose N to be 100 so that the contour length of the swimmer is $L_c = 50a_0$. In order to mimic microorganisms which show propulsion with small amplitude waves, such as nematodes [35] and bull sperms [19,24], we calibrate b to be 0.15 in Eq. (1) so that the amplitude is 10% of the wavelength. To get a directed motion we choose $\kappa/L_c = 5 \times 10^3 k_BT$ so that the mechanical forces are stronger than the thermal forces. A single swimmer in the periodic boundary condition yields a velocity of 0.0025–0.0224 for the respective frequency range of 0.001–0.009, similar to the work of Münch et al. [22]. With these parameters the Taylor lines propagate with the Reynolds number in the range of 0.003–0.028 which is typically seen for microswimmers.

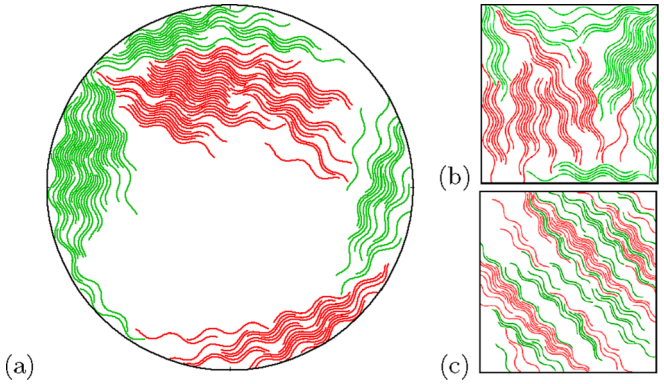

FIG. 1. Snapshots of the stable state of a system with three kinds of boundaries evolved from a random initial state. (a) Circular confinement of $R = 100$ with 150 swimmers, (b) 100×100 square confinement with 75 swimmers, and (c) 150×150 periodic boundary with 110 swimmers. Each system contains a uniform mixture of swimmers with two different beating frequencies ($\delta\nu = 0.1$), $\nu_a = 0.005\,25$ (green) and $\nu_b = 0.004\,75$ (red).

Segregation of bimotility mixture. Yang et al. [23] showed that, if the velocity of each swimmer was chosen from a Gaussian distribution, the cooperation of the swimmers was enhanced when the variance $\sigma < 3\%$. In the present Rapid Communication we analyze a simple system consisting of two types of swimmers which differ from each other only in the swimming speed. Since for a Taylor line the velocity is directly proportional to the beating frequency [22] ν in Eq. (1), we vary the frequency of actuation in our simulations. The beating frequency of the faster swimmers is taken to be ν_a, and that of the slower swimmers is taken to be ν_b. We define $\delta\nu = |\nu_a - \nu_b|/\langle\nu\rangle$ as the relative difference in frequencies. We employ $\delta\nu$ ranging from $10^{-2} - 1$. As the system evolves, the swimmers form aggregations by interacting with the other swimmers via a steric potential [Eq. (2)] and with the fluid through hydrodynamics.

In Fig. 1 we have shown the snapshots as obtained from the simulation for three different boundary conditions where the red color signifies slow swimmers and the green color signifies fast swimmers. In Fig. 1(a) we show the aggregates formed due to the circular rigid boundary condition where we observe that the slow swimmers are usually near the center. A visual inspection reveals that the swimmers have segregated into slow and fast swimmer clusters. In Fig. 1(b) we have shown the aggregate formed due to the rigid square boundary condition where we observe that the faster swimmers are clustering at the corners of the square. Here too a segregation between fast and slow swimmers can be seen. Whereas in Fig. 1(c) we use the periodic boundary condition and observe that the segregation is accompanied by the formation of bands. The Supplemental Material [36], Fig. S1 shows the snapshots of these systems at different time instants.

To quantify the collective behavior, we calculate the cluster size of the swimmers as follows. We consider two swimmers to be part of a cluster if they simultaneously satisfy two conditions for one complete beating period of the faster swimmer. First, if the minimum distance between at least 10% of the beads of the two swimmers is less than $2.27a$, which is the amplitude

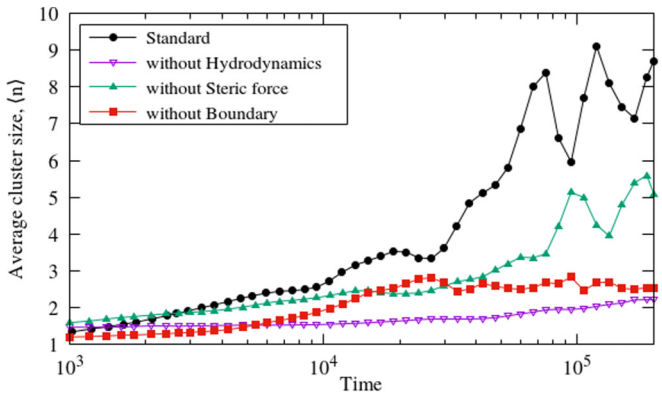

(a)

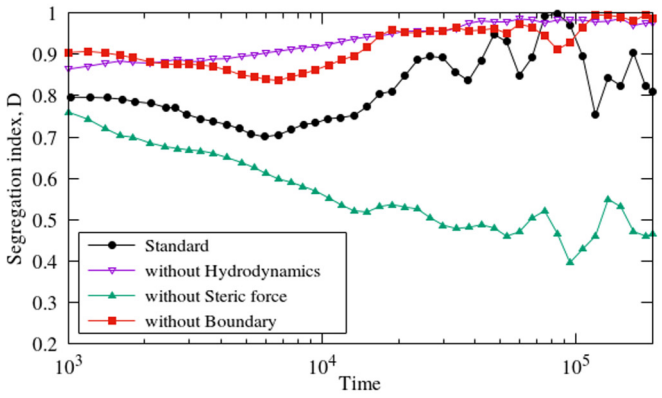

(b)

FIG. 2. Comparison of (a) average cluster size ($\langle n \rangle$) and (b) segregation index (D) vs time of a standard system with circular confinement ($R = 100$) with three similar systems in which the hydrodynamics, the steric force, or the boundary is switched off. In all the systems, $\delta\nu = 0.8$, the average frequency is $\langle \nu \rangle = 0.005$, and the number density of the Taylor lines is $\rho = 0.0048$.

of a swimmer in our case, and second, if the angle between the end-to-end vectors [22] is less than $\pi/6$. See the Supplemental Material [36], Fig. S2 for an illustration of the clusters.

In Fig. 2(a) we show the evolution of the average cluster size $\langle n \rangle = \{\sum n\Pi(n)\}/\sum \Pi(n)$, where $\Pi(n)$ is the cluster size distribution. In the present Rapid Communication a combination of interactions through hydrodynamics, the steric potential, and the boundary leads to clustering and segregation. To perceive the significance of a particular type of interaction, we compare the standard circular boundary system (where all interactions are included) with systems in which hydrodynamic, steric, or boundary interaction is turned off, such that the system parameters are the same. The hydrodynamic interactions are turned off as proposed in Ref. [37] whereas the steric and boundary interactions are turned off by neglecting the force in Eq. (2) and by the periodic boundary condition, respectively. For the standard case, we observe that initially $\langle n \rangle$ increases, signifying that clusters are being formed. These clusters keep on growing until $\langle n \rangle$ reaches a steady state, and then it oscillates around eight indicating there is constant aggregation and fragmentation of the clusters. The increase in $\langle n \rangle$ is not significant in the systems without hydrodynamics or without boundaries as compared to other systems. This implies that steric interactions are not as crucial for clustering as hydrodynamic or boundary interactions. Without the boundary, clusters are in the form of unobstructed parallel bands whereas in a system with a circular boundary, the clusters are able to slide over the walls and collide with other swimmers. This lack of interaction in the periodic boundary condition results in lower $\langle n \rangle$ in the steady state. Likewise, when hydrodynamic interactions are switched off, the swimmers are no longer able to propel themselves to interact with other clusters. Hence, we can infer that the boundaries and hydrodynamics assist in the formation of clusters.

To understand whether we have a segregated state or a mixed state we employ a dimensional number called the segregation index (D) [38],

$$D = \frac{1}{2} \sum_{\text{clusters}} \left| \frac{n_a}{N_a} - \frac{n_b}{N_b} \right|, \tag{3}$$

where $n_{a,b}$ is the population of a or b type swimmers in a particular cluster and $N_{a,b}$ is the total number of a or b type swimmers in the system. The summation runs over all the clusters in the system, which means $D = 1$ implies completely segregated and $D = 0$ implies completely mixed systems. Figure 2(b) illustrates that, for the standard case, D initially increases and reaches 1 signifying a completely segregated state and at later times it oscillates between 0.8 and 1. Also, we observe that when $\langle n \rangle$ is at a maximum D is at a minimum and vice versa. This indicates that, when D is at a minimum, both kinds of swimmers partly mix and form a larger cluster. Then they completely segregate at later times, and therefore we have a minimum in $\langle n \rangle$ and a maximum in D. It has already been shown that a Taylor line always goes towards the rigid wall [22]. In our system, they form clusters close to the wall, and these clusters then start moving along the wall. Even when the system is segregated ($D = 1$) both types of swimmers would eventually encounter each other as we have a circular boundary and one is slower than the other. This can also be seen in the Supplemental Material Movie 1 [36]. In Fig. 2(b) we notice that, except for the system without steric interactions, all the other systems are segregated ($D > 0.7$). Hence, the swimmer-swimmer interactions have leading contributions towards segregating swimmers with different beat wave frequencies.

In the case of the periodic boundary condition, the system interacts with virtual copies of itself, and therefore they form bands which are quite stable. In the rigid square boundary system, the swimmers get stuck at the corners, whereas they are able to slide on the walls in the case of the circular boundary system and interact with other swimmers. Hence, all the results we discuss from here on are for rigid circular boundary conditions only. We have tested systems eight times the area of the system shown in Fig. 1(a) to assert that segregation is observed irrespective of the system size. We also simulated systems in which either the contour length is half or the amplitude is larger by 30% than that used in Fig. 1, snapshots of which are shown in the Supplemental Material [36], Fig. S1. The dynamics is similar even when the length or amplitude of the Taylor line is changed.

Self-organizing dynamics. The cluster size distribution $\Pi(n)$ in the case of circular confinement is plotted in Fig. 3(a).

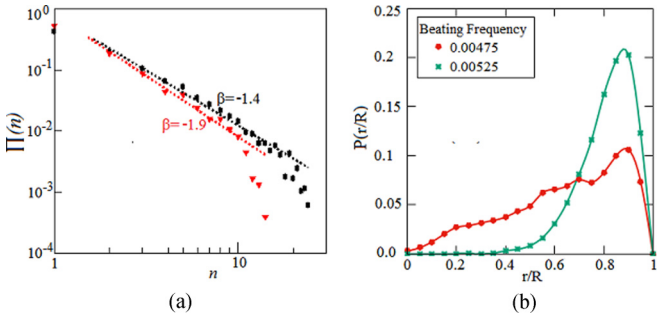

FIG. 3. (a) Time averaged cluster size distribution for two different systems S1 (red) and S2 (black). S1 contains 100 swimmers in 200×200 square confinement, whereas S2 contains 150 swimmers in circular confinement of $R = 100$. Density, $\rho_{S1} = 0.0025$ and $\rho_{S2} = 0.0048$. The curves follow power law decay which breaks down at large values. The data are taken over 12 simulations for various frequencies of swimmers with $\delta\nu$ ranging from 0.005 to 1. (b) The probability of finding a swimmer at a fractional distance r/R from the center, $P(r/R)$ vs r/R for a circularly confined system of $R = 100$ with $\delta\nu = 0.1$.

A power law decay $\Pi(n) \propto n^{\beta}$ is observed for smaller clusters followed by an exponential decay for the higher values of n. The power law exponent β is independent of $\delta\nu$ and the system size and depends only on the density of the swimmers. Figure 3(a) shows β is approximately -1.4 for high density ($\rho = 0.0048$) and approximately -1.9 for low density ($\rho = 0.0025$) similar to what has been reported before for simulations with self-propelled rods [39], spermatozoa [23], and flagella [24] as well as for an experiment with *Myxococcus xanthus* [27]. The distribution is time averaged up to the steady state. We observed that β remains the same even if the time used to average over is increased or decreased by a factor of 2, confirming that it is an inherent property of the system. The decrease in exponent with density shows the importance of interactions for cluster formation. In Fig. 3(b) we have plotted the probability of finding a slow or fast swimmer at a distance r/R from the center of the circle when the system has attained a steady state. Here we notice that the fast swimmers reach the wall earlier and stay near the wall as the distribution is nearly zero towards the center whereas they have sharp peaks close to the walls. In the case of the slow swimmers the distribution is very broad with a very small peak close to the walls. We know that the Taylor lines prefer to be closer to the walls, but when clusters of slower swimmers reach the wall, the faster swimmers fragment and swim through the slow moving cluster. The fragmented segments again move towards the center. See the Supplemental Material Movie 1 [36].

The power laws suggest intermittent behavior in cluster dynamics [39] resulting from aggregation and fragmentation at the steady state. To quantify the contribution of the fast and slow swimmers towards cluster formation we introduce a parameter η defined as

$$\eta_{a,b} = \frac{\sum \left(\frac{n_{a,b}}{n}\right) \Pi(n)}{\sum \Pi(n)}, \tag{4}$$

which gives the contribution of either an a or b swimmer in a cluster of size n. The time dependence of η is plotted in Fig. 4

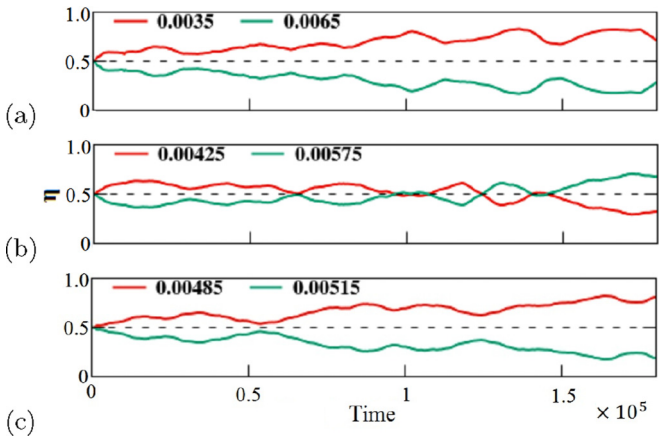

FIG. 4. η_a and η_b vs time for three systems having circular confinement with $R = 100$. For all systems, $N_a = N_b = 75$. The systems differ only in the beating frequency of the swimmers, (a) $\delta\nu_1 = 0.6$, (b) $\delta\nu_2 = 0.3$, and (c) $\delta\nu_3 = 0.06$. The $\langle\nu\rangle$ in all three cases is 0.005. The segregation index for these systems is plotted in the Supplemental Material [36], Fig. S3.

for the time period before the system reaches a steady state. We can observe that the contribution of slower swimmers to the clusters is higher than that of the faster swimmers. In Fig. 4 we have plotted the evolution of $\eta(a)$ and $\eta(b)$ for three different values of $\delta\nu$. It can be seen that, for both large and small values of $\delta\nu$, the values of η_b are always above 0.5 and the values of η_a are below 0.5. For the large difference in $\delta\nu$ the slower swimmers contribute more for the cluster formation, whereas the faster swimmers prefer to form smaller clusters. As $\delta\nu$ is reduced to an intermediate value, i.e., $\delta\nu = 0.2$, η_a and η_b fluctuate around 0.5, i.e., the contribution towards the cluster by both swimmers is almost the same. If we further decrease $\delta\nu$, we again observe that the contribution of the slower swimmers is much more than the faster swimmers.

In the present Rapid Communication thus we are able to observe three different regions based on the clustering of swimmers. Figure 5 shows a time average of $\langle\eta\rangle$ for the

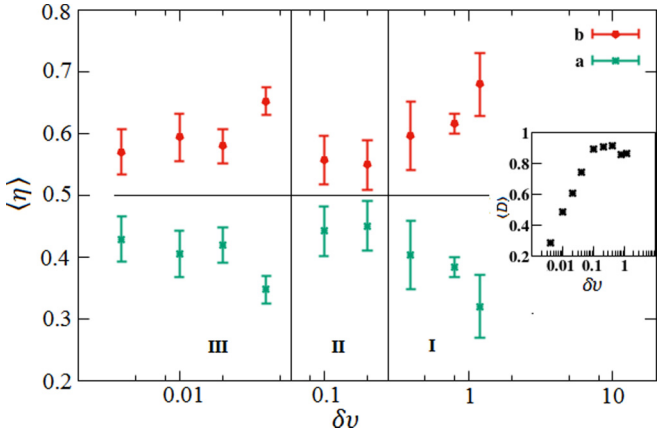

FIG. 5. The time average of η plotted vs $\delta\nu$. The data are averaged over systems with circular confinement varying in R and $\langle\nu\rangle$. The mixtures are homogeneous with number density $\rho \approx 0.005$. The inset shows the time average of segregation index vs $\delta\nu$. The average is taken over the simulation period.

whole simulation period vs $\delta\nu$. Each point is averaged over six different configurations with $\rho \approx 0.005$. In region I, the faster ones push through the slower ones to reach the walls in small clusters, whereas the slower ones are at that time dispersed around the center of the system. As a result, the segregation index as apparent from the inset of Fig. 5 and the Supplemental Material [36], Fig. S3 is greater than 0.8 and $\langle \eta_b \rangle > 0.5$. Whereby, the suspended slower ones easily form clusters at the center of the circular confinement. With the decrease in difference in beating frequency of swimmers in region II, the fast swimmers are unable to push through, and there is virtually a competition between both kinds of swimmers to form clusters in the confinement. As a result, on average, there is almost an equal contribution from both kinds to cluster, and thus $\langle \eta_b \rangle$ tends to 0.5. If $\delta\nu$ is decreased further in region III, both kinds of swimmers easily form clusters with each other as $\langle D \rangle < 0.8$. $\langle \eta_b \rangle > 0.5$ suggests that the concentration of slower swimmers is higher in a cluster and the slow ones exploit the thrust of the fast swimmers to form clusters. Thus the faster swimmers are always leading inside a cluster, whereas there is a high density of slower swimmers at the back of the cluster. See the Supplemental Material Movie 2 [36]. Gradually, the faster swimmers start swimming out of the cluster thereby increasing the segregation. Thus, the parameter $\delta\nu$ plays an important role in controlling the cluster dynamics of the system. We have also simulated systems with $\delta\nu = 0.004$ to observe that, as $\delta\nu$ tends to zero, η and $\langle D \rangle$ tend to 0.5 and zero, respectively, as expected.

Conclusion. For the Taylor lines in confinement, we have shown that the cooperation in a bimotility mixture of swimmers involves distinct interactions which result in their aggregation along with segregation into faster and slower ones. The interactions with the fluid and the boundary primarily assist in aggregation, whereas the swimmer-swimmer interactions induce segregation of the mixture. The tendency of segregation has been reported in experiments [2,5,11,13] in which such binary mixtures are developed artificially or in natural response to external stimuli and in recent simulations of active and passive particles [31,32,40,41]. However, we have shown that the system shows different behaviors depending on the relative difference in speed. The results can be exploited to understand the collective dynamics among microswimmers in real systems which are composed of a continuous distribution of motility. We can infer that a stable cluster of swimmers is composed of those with small differences in ν in which the slower ones are at the back guided by small numbers of the faster ones, which is also observed experimentally [1,9]. When the difference in ν between clusters is large, the faster ones move away from the center assisting efficient swarming which has also been reported in the study of mixtures of healthy and dying microorganisms [2,11,13]. Our simulations reveal the novel kinds of cooperation between different microswimmers which stimulate the collective motion in a suspension.

Acknowledgments. We would like to acknowledge the HPC cluster at IIT Delhi, as well as baadal, IITD's private cloud, for allowing us to use the facility for the purpose of running the simulations.

[1] T. Vicsek and A. Zafeiris, Phys. Rep. **517**, 71 (2012).
[2] S. Benisty, E. Ben-Jacob, G. Ariel, and A. Be'er, Phys. Rev. Lett. **114**, 018105 (2015).
[3] Y. Wu, Y. Jiang, D. Kaiser, and M. Alber, PLoS Comput. Biol. **3**, e253 (2007).
[4] J. Elgeti, R. G. Winkler, and G. Gompper, Rep. Prog. Phys. **78**, 056601 (2015).
[5] S. Ramaswamy, Annu. Rev. Condens. Matter Phys. **1**, 323 (2010).
[6] J. Stenhammar, C. Nardini, R. W. Nash, D. Marenduzzo, and A. Morozov, Phys. Rev. Lett. **119**, 028005 (2017).
[7] G. Li and A. M. Ardekani, Phys. Rev. Lett. **117**, 118001 (2016).
[8] A. Zöttl and H. Stark, Phys. Rev. Lett. **112**, 118101 (2014).
[9] M. Aureli and M. Porfiri, in *ASME 2011 Dynamic Systems and Control Conference and Bath/ASME Symposium on Fluid Power and Motion Control, Arlington, VA, 2011* (ASME, New York, 2011), Vol. 1, pp. 9–16.
[10] J. Blaschke, M. Maurer, K. Menon, A. Zöttl, and H. Stark, Soft Matter **12**, 9821 (2016).
[11] D. B. Kearns, Nat. Rev. Microbiol. **8**, 634 (2010).
[12] E. Lauga and T. R. Powers, Rep. Prog. Phys. **72**, 096601 (2009).
[13] N. C. Damton, L. Turner, S. Rojevsky, and H. C. Berg, Biophys. J. **98**, 2082 (2010).
[14] M. Oberholzer, M. A. Lopez, B. T. McLelland, and K. L. Hill, PLoS Pathog. **6**, e1000739 (2010).
[15] P. Malgaretti and H. Stark, J. Chem. Phys. **146**, 174901 (2017).
[16] S. B. Babu and H. Stark, New J. Phys. **14**, 085012 (2012).
[17] T. Majmudar, E. E. Keaveny, J. Zhang, and M. J. Shelley, J. R. Soc., Interface **9**, 1809 (2012).
[18] S. B. Babu and H. Stark, Eur. Phys. J. E **34**, 1 (2011).
[19] J. Gray and G. J. Hancock, J. Exp. Biol. **32**, 802 (1955).
[20] G. Taylor, Proc. R. Soc. London, Ser. A **209**, 447 (1951); T. R. Powers, Rev. Mod. Phys. **82**, 1607 (2010).
[21] G. J. Elfring and E. Lauga, Phys. Rev. Lett. **103**, 088101 (2009).
[22] J. L. Münch, D. Alizadehrad, S. Babu, and H. Stark, Soft Matter **12**, 7350 (2016).
[23] Y. Yang, J. Elgeti, and G. Gompper, Phys. Rev. E **78**, 061903 (2008).
[24] Y. Yang, V. Marceau, and G. Gompper, Phys. Rev. E **82**, 031904 (2010).
[25] B. Liebchen, D. Marenduzzo, I. Pagonabarraga, and M. E. Cates, Phys. Rev. Lett. **115**, 258301 (2015).
[26] B. Liebchen, D. Marenduzzo, and M. E. Cates, Phys. Rev. Lett. **118**, 268001 (2017).
[27] F. Peruani, J. Starruß, V. Jakovljevic, L. Søgaard-Andersen, A. Deutsch, and M. Bär, Phys. Rev. Lett. **108**, 098102 (2012).
[28] O. Pohl and H. Stark, Eur. Phys. J. E **38**, 93 (2015).
[29] O. Pohl and H. Stark, Phys. Rev. Lett. **112**, 238303 (2014).
[30] S. R. McCandlish, A. Baskaran, and M. F. Hagan, Soft Matter **8**, 2527 (2012).
[31] J. Stenhammar, R. Wittkowski, D. Marenduzzo, and M. E. Cates, Phys. Rev. Lett. **114**, 018301 (2015).

[32] J. Smrek and K. Kremer, Phys. Rev. Lett. **118**, 098002 (2017).
[33] A. Malevanets and R. Kapral, J. Chem. Phys. **110**, 8605 (1999).
[34] G. Gompper, T. Ihle, D. M. Kroll, and R. G. Winkler, Adv. Polym. Sci. **221**, 1 (2009).
[35] C. J. Cronin, J. E. Mendel, S. Mukhtar, Y.-M. Kim, R. C. Stirbl, J. Bruck, and P. W. Sternberg, BMC Genet. **6**, 5 (2005).
[36] See Supplemental Material at http://link.aps.org/supplemental/10.1103/PhysRevE.97.020401 for movie captions and more figures.
[37] M. Ripoll, R. G. Winkler, and G. Gompper, Eur. Phys. J. E **23**, 349 (2007).
[38] O. D. Duncan and B. Duncan, Am. J. Sociol. **60**, 493 (1955).
[39] C. Huepe and M. Aldana, Phys. Rev. Lett. **92**, 168701 (2004).
[40] A. Awazu, Phys. Rev. E **90**, 042308 (2014).
[41] S. N. Weber, C. A. Weber, and E. Frey, Phys. Rev. Lett. **116**, 058301 (2016).